Title

Development of Novel Tumor-Targeted Theranostic Nanoparticles Activated by Membrane-Type Matrix Metalloproteinases for Combined Cancer Magnetic Resonance Imaging and Therapy

Journal

Small, 10(3)

ISSN

1613-6810

Authors

Ansari, Celina
Tikhomirov, Grigory A
Hong, Su Hyun
et al.

Publication Date

2014-02-01

DOI

10.1002/smll.201301456

Peer reviewed

Published in final edited form as:
Small. 2014 February 12; 10(3): 566–417. doi:10.1002/smll.201301456.

Development of Novel Tumor-Targeted Theranostic Nanoparticles Activated by Membrane-Type Matrix Metalloproteinases for Combined Cancer Magnetic Resonance Imaging and Therapy

Dr. Celina Ansari[=],
Molecular Imaging Program at Stanford, Stanford University, 725 Welch Road, Rm 1665, Stanford, CA 94305-5614 USA

Dr. Grigory A. Tikhomirov[=],
Molecular Imaging Program at Stanford, Stanford University, 725 Welch Road, Rm 1665, Stanford, CA 94305-5614 USA

Su Hyun Hong,
Molecular Imaging Program at Stanford, Stanford University, 725 Welch Road, Rm 1665, Stanford, CA 94305-5614 USA

Dr. Robert A. Falconer,
Institute of Cancer Therapeutics, School of Life Sciences, University of Bradford, Richmond Road, Bradford BD7 1DP. UK

Dr. Paul M. Loadman,
Institute of Cancer Therapeutics, School of Life Sciences, University of Bradford, Richmond Road, Bradford BD7 1DP. UK

Dr. Jason H. Gill,
School of Medicine, Pharmacy and Health, Durham University, Queens Campus, Stockton-on-Tees, TS17 6BH. UK

Rosalinda Castaneda,
Molecular Imaging Program at Stanford, Stanford University, 725 Welch Road, Rm 1665, Stanford, CA 94305-5614 USA

Prof. Florette K. Hazard,
Department of Pathology, Stanford University, 300 Pasteur Drive, Stanford, CA 94305 USA

Dr. Ling Tong,
Division of Oncology, Department of Medicine, Stanford University, 269 Campus Drive, CCSR 1105, Stanford, CA 94305 USA

Olga D. Lenkov,

Corresponding Authors: Prof. H.E. Daldrup-Link and Prof. J. Rao, Molecular Imaging Program at Stanford, Stanford University, 725 Welch Road, Rm 1665, Stanford, CA 94305-5614 USA, heiked@stanford.edu or jrao@stanford.edu.
[=]Both authors contributed equally to this study
[*]Authors are co-last authors

Supporting Information is available on the WWW under http://www.small-journal.com or from the author.

Molecular Imaging Program at Stanford, Stanford University, 725 Welch Road, Rm 1665, Stanford, CA 94305-5614 USA

Prof. Dean W. Felsher,
Department of Pathology, Stanford University, 300 Pasteur Drive, Stanford, CA 94305 USA. Division of Oncology, Department of Medicine, Stanford University, 269 Campus Drive, CCSR 1105, Stanford, CA 94305 USA

Prof. Jianghong Rao, and
Molecular Imaging Program at Stanford, Stanford University, 725 Welch Road, Rm 1665, Stanford, CA 94305-5614 USA

Prof. Heike E. Daldrup-Link*
Molecular Imaging Program at Stanford, Stanford University, 725 Welch Road, Rm 1665, Stanford, CA 94305-5614 USA

Abstract

A major drawback with current cancer therapy is the prevalence of unrequired dose-limiting toxicity to non-cancerous tissues and organs, which is further compounded by a limited ability to rapidly and easily monitor drug delivery, pharmacodynamics and therapeutic response. In this report, we describe the design and characterization of novel multifunctional "theranostic" nanoparticles (TNPs) for enzyme-specific drug activation at tumor sites and simultaneous *in vivo* magnetic resonance imaging (MRI) of drug delivery.

TNPs were synthesized by conjugation of FDA-approved iron oxide nanoparticles ferumoxytol to an MMP-activatable peptide conjugate of azademethylcolchicine (ICT), creating CLIO-ICTs (TNPs). Significant cell death was observed in TNP-treated MMP-14 positive MMTV-PyMT breast cancer cells *in vitro*, but not MMP-14 negative fibroblasts or cells treated with ferumoxytol alone. Intravenous administration of TNPs to MMTV-PyMT tumor-bearing mice and subsequent MRI demonstrated significant tumor selective accumulation of the TNP, an observation confirmed by histopathology. Treatment with CLIO-ICTs induced a significant antitumor effect and tumor necrosis, a response not observed with ferumoxytol. Furthermore, no toxicity or cell death was observed in normal tissues following treatment with CLIO-ICTs, ICT, or ferumoxytol.

Our findings demonstrate proof of concept for a new nanotemplate that integrates tumor specificity, drug delivery and *in vivo* imaging into a single TNP entity through attachment of enzyme-activated prodrugs onto magnetic nanoparticles. This novel approach holds the potential to significantly improve targeted cancer therapies, and ultimately enable personalized therapy regimens.

Keywords

nanoparticles; iron oxide; cancer therapy; MR imaging, theranostic; MMP-14

1. Introduction

Current cancer therapies commonly involve radiation and cytotoxic chemotherapeutic treatment, both of which generate serious toxic side effects. Mechanistically these treatments

do not exclusively target cancer cells, but also damage proliferating cell types of the digestive tract, central nervous system and bone marrow, and physiological functions of many tissues, commonly resulting in toxicities and impaired organ function. Therefore, there is an urgent need for novel approaches to selective targeting therapeutics to tumors.

A number of drug-loaded nanocarrier systems have been evaluated for this goal, and their accumulation at the tumor site is primarily achieved by "passive targeting" via exploitation of the proposed enhanced permeability and retention (EPR) effect in tumors.[1] The use of nanoparticles has been shown to significantly increase blood circulation time and improve tumor retention of several chemotherapeutics, overcoming the sub-optimal pharmacokinetics and toxicity profiles associated with many of these agents.[1c, 2] However, this approach relies upon tumor pathophysiology for extravasation and the highly heterogeneous nature of the EPR effect, which can lead to poor clinical efficacy.[1b, 1c] Alternatively, these drug-loaded nanotherapeutics may be actively targeted to the tumor with ligands against a receptor overexpressed at the tumor cell surface to improve uptake and retention in tumor cells, although the initial tumor accumulation is still EPR dependent. [1c, 3] An emerging strategy in cancer therapy utilizes therapeutic agents that selectively target the tumor vasculature, resulting in an indirect antitumour effect.[4] These *vascular disrupting agents* (VDAs) selectively destabilize tumor endothelium causing an increase in vascular permeability and collapse of intratumoral blood vessels[4–5] thereby inducing a temporal enhancement of the EPR effect. Consequently, the actions of VDAs can therefore function to both enhance drug targeting and retention at the tumor site. Thus tumor vasculature-targeted nanotherapeutics should be more efficacious than conventional nanotherapeutics because they do not rely on extravasation or penetration across several cell layers for activity, would have direct contact with their target endothelial cells, and can be designed to dose-intensify therapeutics at the tumor site. Furthermore, it is now well established that the disruption of a single tumor blood vessel has the additional effect of starving and consequently killing the tumor cells it supports, making this a very effective therapeutic strategy.[4b, 6] However, it is becoming increasingly apparent that the therapeutic value of VDAs is compromised by their intrinsic toxicity, particularly the induction of cardiac ischemia and arrhythmias.[7] Therefore, an improved strategy would be to deliver a nanotherapeutic that is nontoxic systemically but selectively converted to an active vascular-targeted agent within the tumor tissue, thereby allowing selective destruction of tumor-associated blood vessels and tumor cells without impairing non-neoplastic cells in normal organs.

To convert systemically nontoxic prodrugs to toxic therapeutics in malignant tissue requires the exploitation of enzymes elevated selectively in the tumor microenvironment.[8] One such family of enzymes is the matrix metalloproteinases (MMPs) because of their markedly significant elevated expression in human cancer tissues and ability to selectively cleave specific peptide sequences.[8–9] Among the large family of MMPs, the membrane-type MMP (MT-MMP) subclass has been suggested to play dominant roles in controlling invasive cancer cell behavior.[10] In particular, MMP-14 (MT1-MMP) not only plays a direct and essential role in allowing tumor cells to invade into connective tissue,[11] but also provides a direct cellular target for prodrug activation.[10] Recently, Atkinson *et al.* demonstrated that an MMP-14 peptide substrate conjugate of azademethylcolchicine, a highly potent vascular disrupting agent, was selectively activated by MMP-14 at the tumor

site.[12] In this work, we linked the azademethylcolchicine prodrug to a nanocarrier, FDA-approved superparamagnetic iron oxide nanoparticles, through the MMP-14 cleavable peptide substrate and generated a nanotherapeutic activated by tumor specific MMP-14 for tumor vascular targeting.

A further issue with current cancer treatments is the limited ability to initially evaluate the level of disease dissemination, and then subsequently monitor the delivery and efficacy of therapeutics. Combinations of nanocarriers with different imaging contrast agents have led to the development of platforms for single and multimodal tumor imaging, permitting detection of smaller lesions and monitoring of disease dissemination and progression.[1a] Similarly, several activatable probes for cancer detection with clinically applicable imaging modalities, such as MR, have been described,[13] but these nanocarriers loaded with contrast agents generally lack anticancer activity.[1a] Progress in molecular imaging methodologies and recent advances in nanomedicine technologies have made it possible for the development of multifunctional "theranostic" nanoparticles (TNPs) that combine targeted therapeutics and diagnostic functionality into the same agent.[1a, 1d, 14]

In this study, we have integrated two proven technologies: a tumor MMP-14 activatable prodrug strategy[12] and an iron oxide nanocarrier platform to develop activatable "theranostic" nanoparticles (termed CLIO-ICT or TNPs). CLIO-ICT is composed of FDA-approved superparamagnetic iron oxide nanoparticles, linked to an MMP-14 cleavable peptide-conjugate of azademethylcolchicine.[12] The use of iron oxide nanocarriers allows CLIO-ICT to be imaged *in vivo* by clinically applicable MRI technologies,[15] which provides direct quantitation and imaging of the delivery of CLIO-ICT to tumors. We hypothesize that CLIO-ICT will be converted from a non-toxic to an active agent within MMP-14 expressing tumors, releasing the potent vascular disrupting agent, azademethylcolchicine. The action of azademethylcolchicine to cause a rapid conformational change in the tumor vasculature, increased vascular permeability and subsequent vascular collapse[4b, 5] will also aid retention and entrapment of the TNPs within the tumor. This strategy should therefore allow real-time monitoring of drug accumulation and localization at tumors with MR imaging and induce a significant antitumor effect, whilst avoiding toxic side effects to normal tissues. We expect that these multifunctional TNPs hold the potential to improve the efficacy of targeted cancer therapies, and guide personalized therapy regimens via direct *in vivo* drug tracking and therapeutic response monitoring with MR maging.

2. Results

2.1. Design of TNPs

The concept for MMP-14 activatable TNPs (CLIO-ICT) is shown in Figure 1, and the molecules consist of three main elements: (i) core, (ii) linker, and (iii) drug. These TNPs are comprised of the following: (i) The core is a cross-linked iron oxide (CLIO) nanoparticle with an ultra-small (6.5 nm) iron oxide crystal encapsulated into an 8 nm thick polysaccharide dextran shell. Superparamagnetism of the core allows for MR imaging of the TNP. (ii) The linker is an MMP-14 peptide recognition sequence with an *N*-terminal masking group containing fluorescein: FITC-βAla-Cys-Arg-Ser-Cit-Gly-HPhe-Tyr-Leu-Tyr

that is specifically cleaved between glycine and homophenylalanine (HPhe) by tumor-associated MMP-14.[12] (iii) The drug is azademethylcolchicine. The amino group of azademethylcolchicine was attached to the peptide, thereby rendering the drug non-toxic until activated, as demonstrated previously for the MMP-activated prodrug ICT2588.[12] The fluorescent masking group enables physicochemical characterization and therefore serves as a label for TNPs, in addition to its role in providing metabolic stability to the peptide.[12]

2.2. Physicochemical Properties of TNPs

CLIO-ICT was characterized by Dynamic Light Scattering (DLS), Laser Doppler Electrophoresis, UV-Vis absorption spectroscopy, fluorescence spectroscopy, and Nuclear Magnetic Resonance (Table 1). DLS measurements showed the expected increase in the NPs size from 19 nm to 21 nm after conjugation with ICT. Cross-linking, amine group addition, and ICT attachment also changed the charge of the nanoparticle: it was negative for ferumoxytol, positive for both CLIO-ICT and its MMP-14 cleavage product according to laser Doppler electrophoresis (zeta potential measurements, Table 1). The number of ICT molecules per iron oxide nanoparticle was determined to be on average 4.7 from the attached fluorescein absorption and known TNP concentration.

TNP activation was studied using HPLC to analyze solutions of both ICT (10 mM) and CLIO-ICT (10 mM) post-incubation with recombinant MMP-14 (20 μg/mL) in PBS buffer at 37 °C (Figure 2). One of the major peptide metabolites identified by mass spectrometry (HPhe-Tyr-Leu-Tyr-azademethylcolchicine) was identical to the one previously reported for the original ICT2588 prodrug,[12] confirming that the two molecules have similar cleavage profiles. It was previously shown that this cleavage fragment is subsequently metabolized rapidly in the tumor by exopeptidases in a non-specific manner to release the active drug.[12] The chosen length of the linker (2.6 nm, calculated in Chem3D Ultra 8.0) was sufficient for efficient cleavage: MMP-14 cleaved the peptide linker and released 87% of the total calculated quantity of ICT after 2 hours as measured by absorption spectra (almost no characteristic absorption of ICT in absorption spectra after cleavage). MMP-14 treatment of ICT in identical conditions cleaved 89% of the prodrug as was observed by HPLC assays.

The size of the TNPs decreased slightly upon cleavage by MMP-14 as measured by DLS (Table 1). As expected, the iron oxide core size did not change upon functionalization (6.5±0.7 after functionalization versus 6.2–7.3 before[16]) as determined by Transmission Electron Microscopy (TEM; Table 1). Modified TNPs had slightly higher r1's (33.9 for CLIO-ICT and 39.5 $mM^{-1}s^{-1}$ for the cleaved CLIO-ICT) and lower r2's (56.0 for CLIO-ICT and 55.8 $mM^{-1}s^{-1}$ for the cleaved CLIO-ICT) compared to original ferumoxytol nanoparticles (32.3 and 74.9 $mM^{-1}s^{-1}$, respectively), which is likely due to the increase in molecular weight and the nature of the coating.

2.3. Anticancer Activity of TNPs *In Vitro*

qPCR revealed significant MMP-14 expression in MMTV-PyMT tumor cells, while 4T1 tumor cells and fibroblasts did not show significant MMP-14 expression (Figure 3B). Expression data were collected as Ct values and the gene expression levels were normalized

to the reference control gene, GAPDH. MMTV-PyMT tumor cells showed significant cell death after incubation with CLIO-ICT (caspase expression ratio of 2.883:1 relative to the PBS control) and ICT (caspase expression ration of 2.994:1 relative to the PBS control), but not after incubation with ferumoxytol (1.47:1) and PBS control (1:1). 4T1 cells were not responsive to treatment with CLIO-ICT and MMP-14 negative fibroblasts did not show any significant cytotoxic effects after incubation with CLIO-ICT or ICT (Figure 3A).

In addition we found that activation of the drug was in fact due to MMP-14 dependent cleavage of the probe by performing a set of MMP blocking experiments with Ilomostat, which showed the disapperance CLIO-ICT and ICT antitumor activities (Figure S5).

2.4. Tumor Accumulation of TNP *In Vivo*

After a single intravenous injection of ferumoxytol (0.5 mmol Fe/kg) and CLIO-ICT (0.75 mmol Fe/kg), MMTV-PyMT tumors demonstrated a negative (dark) enhancement on postcontrast T2-weighted MR images (Figure 4). This negative tumor enhancement persisted for the entire time period of observation, up to 24 h post-injection. Tumor enhancement with TNPs was not significantly different compared to the tumor enhancement with the original, "diagnostic" nanoparticle ferumoxytol (Figure 4). Control mice injected with the therapeutic ICT or injected with PBS did not show any significant MR signal enhancement (Figure 4). This result confirmed that the evaluated MMTV-PyMT tumors did not exhibit any intrinsic changes in MR signal within a two-day observation period and that ICT did not cause any MR signal changes either. Detection of iron using DAB-enhanced Prussian Blue staining and immunostaining of TNP-FITC with Alexa 488 conjugated anti-FITC antibody confirmed accumulation of TNPs and ferumoxytol in MMTV-PyMT tumors (Figure 5). Accumulation of TNPs in the tumor was also monitored by measuring the fluorescence of fluorescein which is the part of both CLIO-ICT and ICT. TNP showed higher fluorescence intensity in the tumor at all times which is likely to be due to a higher accumulation of CLIO-ICT relative to ICT (Figure S4).

2.5. Antitumor Activity of TNPs *In Vivo*

Daily monitoring of MMTV-PyMT tumor size indicated that PBS and ferumoxytol treated subjects showed an increase in tumor size (P=0.002) whereas those treated with CLIO-ICT and ICT showed an overall decrease in tumor size (P=0.002, Figure 3). Pathologic evaluation of tumors confirmed a progressive increase in the severity of tumor necrosis following ICT or CLIO-ICT treatment (Figure 5). In contrast, no significant tumor necrosis was observed in ferumoxytol treated tumors (Figure 5). An analogous pattern of progressive cellular cytotoxicity was observed with the Cy3-labeled cleaved Caspase-3 immunofluorescent staining: there was rare labeling of tumor cells for the ferumoxytol injected mice, but significant labeling of tumor cells from both the ICT and CLIO-ICT treated mice (Figure 5). Iron deposits were noted within ferumoxytol and CLIO-ICT treated groups, but not in PBS or ICT-treated groups (Figure 5).

Conversely, no significant toxicity was observed in normal organs (liver, spleen, kidney, brain, bone marrow and heart), detected either histologically, by detection of caspase-3 activity (Figure 6), and animal weight loss (Figure S3). In addition we monitored the

stability of CLIO-ICT and ICT in mouse blood and found no ICT cleavage products by mass-spectrometry.

3. Discussion

The effectiveness and success of current cancer chemotherapy is hindered by undesired dose-limiting toxicity to non-cancerous tissues and organs. In addition, treatment response monitoring is restricted by a lack of tools for rapidly and non-invasively monitoring drug delivery and pharmacokinetics. Approaches to improving therapeutic efficacy and monitoring whilst simultaneously reducing dose-limiting toxicities, thereby increasing the therapeutic index, are a very attractive strategy for development of cancer therapeutics. Consequently, we have developed and preliminarily evaluated in vivo an MMP-14 activatable theranostic agent as a novel approach to the tumor-selective delivery and imaging of a potent vascular-disrupting agent.

The concept of theranostic nanoparticles (TNPs) was originally developed to exploit the hyperpermeable vasculature of cancer, which is not found in normal tissues, a principle termed the EPR effect. This strategy, although highly effective preclinically, has not yet attained the proposed potential bestowed by the success of nanoparticle-based diagnostic imaging, with limitations being attributed to tumor pathophysiology and the highly heterogeneous nature of the EPR effect.[1b, 1c] Although recently, TNPs have been suggested as an aid to this obstacle through their ability to non-invasively report the degree of EPR effect present within a tumor.[17] One reported limitation of TNPs is that although they do not extravasate across intact vascular endothelia, they are known to extravasate across organs of the reticuloendothelial system (RES) containing microvessels with sinusoids.[18] It is therefore recognized that strategies are required to enhance tumor-selective delivery and reduce potential for toxic side effects in the RES system. Previously, activatable MR probes for cancer imaging have been described,[1d, 13, 19] but as probes they clearly lack the anticancer activity that a "theranostic" can provide. Among activatable previously described cancer TNPs,[20] [17] many exhibit fluorescence upon activation, which has limited signal tissue penetration or intrinsic toxicity (e.g. heavy metals in quantum dots). Several strategies have been previously investigated for tumor-selective delivery, such as diffusion from a vesicle/micelle and pH activated drug release, many of which have been largely unsuccessful.[1c, 20c, 20f, 21] Other approaches have relied upon attachment to an active tumor-cell targeting ligand such as folate or RGD.[1a, 22] The activation system in our TNPs is "builtin" and does not require external stimuli for release of the drug such as near-infrared light, radiofrequency ablation, or magnetic thermal induction,[20g] relying instead upon tumor-associated MMP-14 activation.

A further complication with other theranostic strategies is that their therapeutic mechanism invariably requires the drug to interact with cells within the tumor mass, which can be several cell layers thick. Our strategy uses tumor vasculature-disrupting agents (VDAs), specifically azademethylcolchicine, rather than 'conventional' anticancer agents such as the anthracyclines or antimetabolites. Mechanistically, VDAs target tumor endothelia providing an added advantage that they cause direct damage to the vasculature resulting in vessel

collapse and a cessation of blood flow within the tumor,[4b, 6] and are not required to penetrate throughout the tumor mass or directly interact with tumor cells.

Our theranostic strategy builds on the previous development of ICT2588, a novel MMP-14-activated tumor-targeted VDA, which showed tumor-selective activation and significant therapeutic efficacy with demonstrated potential for circumventing systemic toxicity.[12] The therapeutic study described herein has progressed and advanced this strategy by linking this concept to a magnetic nanoparticle to create the theranostic agent CLIO-ICT. This provided the opportunity to monitor and potentially enhance therapeutic efficacy, with the key advances being the ability to identify tumor localization and disease extent, and simultaneously evaluate and visualize the *in vivo* tumor accumulation of the therapeutic with MR imaging, which is not possible with ICT that is not bound to an imaging NP.

We showed MMP-14 hydrolysis of CLIO-ICT to liberate the correct proteolytic-VDA fragment through cleavage at the glycine-homophenylalanine bond, and differential *in vitro* chemosensitivity in MMTV-PyMT (high MMP-14) but not in 4T1 (low MMP-14) tumor cells or normal fibroblasts. To check TNPs off-site activation, we performed both HPLC and LC-MS search for cleavage products including Colchicine-Tyr-Leu-Tyr-Hof (shown in Figure 2C), Colchicine-Tyr-Leu-Tyr, Colchicine-Tyr-Leu, Colchicine-Tyr, and Colchicine, and their fragmentation products. As shown in Figure S7, under the same incubation and elution conditions, TNP incubated with blood didn't produce the Colchicine-Tyr-Leu-Tyr-Hof peak- –one of the MMP-14 cleavage products. MS analysis of all other peaks did not reveal any matches with the potential cleavage products listed above. This in vitro result is consistent with the observed systematic stability and tumor-selective accumulation of CLIO-ICT in mouse models.

The nanoparticle component of our CLIO-ICT drug was utilized to monitor TNP tumor accumulation *in vivo* with MR imaging. As shown by our data, MR signal effects correlated with TNP tumor accumulation. The reviewer raises an important point, that our imaging technique does not visualize the activation of our TNP. The TNPs could be further refined so that tumor-selective drug release could be imaged in real time. Currently, differences in r1 and r2 relaxivities between the original CLIO-ICT and activated products are too small to be visualized by MRI in vivo (50.0 versus 55.8 $mM^{-1}s^{-1}$). Future generations of TNPs could produce MRI contrast either during drug-activation or as a consequence of the drugs pharmacological activity, to facilitate monitoring of drug release kinetics. This may be done by attaching 2-cyano-6-aminobenzothiazole (CABT) and S-ethyl-cysteine moieties that after a loss of S-ethyl fragment and MMP peptide cleavage will cause a biocompatible condensation reaction between CABT and cysteine, which leads to aggregation of TNPs and in turn increases R_2 contrast.

Conjugation of ICT to the NP did not diminish the MMP-14 dependent anticancer efficacy of the prodrug as significant hemorrhagic necrosis was observed in the tumor following administration. This mechanism is consistent with VDA-induced decrease in functional tumor vasculature, a pharmacodynamic effect observed for ICT2588 and other VDA approaches.[6, 12] Additionally, no antitumor effect or tumor response was observed in the ferumoxytol (NP) treated mice, which suggests that the therapeutic effect is derived directly

from the released VDA entity. Most importantly for this approach and as suggested by the previous study with ICT2588,[12] there was a lack of detectable toxicity and MR signal in non-tumor tissues, strongly supporting the tumor-selective toxicity and widespread potential of this strategy. Further studies have to evaluate the respective contribution of MMP-14 expression by invasive tumor cells, angiogenic blood vessels and dynamic tumor stroma to the activation and therapeutic effects of our TNPs.

4. Conclusion

CLIO-ICT demonstrated both significant MR imaging effects and anticancer activity, with selective and effective delivery to the tumor site, and with consecutive reduction of associated toxicity-liability to normal organs. In addition, the conjugation of a therapeutic to nanoparticles allows for a significantly higher drug payload to be delivered. The advantages of our CLIO-ICT nanotherapeutics include the ability to track the drug with MRI, together with longer retention in the tumor tissue via VDA-initiated vascular collapse and drug entrapment, and improved antitumor efficacy. Conceptually this is important, as by noninvasively visualizing how well our TNP accumulates at the target site, patient response to TNP treatment may be preselected. With further validation studies, this TNP approach may also allow longitudinal monitoring of patient response, allowing drug doses and treatment protocols to be individualized and optimized during follow-up. Consequently, the TNP approach holds significant potential for improving the targeted therapy of cancers, and personalized nanomedicine based chemotherapeutic interventions, to achieve delivery of the right drug to the right location in the right patient at the right time.[17]

5. Experimental Section

5.1. Synthesis of TNPs

For the synthesis of TNPs, we used the ultrasmall superparamagnetic iron oxide nanoparticle compound (USPIO) ferumoxytol, an FDA-approved iron supplement for intravenous treatment of iron deficiency.[11, 16, 23] Ferumoxytol consists of an iron oxide core and a carboxymethyldextran coating. The carboxydextran coated ferumoxytol nanoparticles were first cross-linked with epichlorohydrin for better stability *in vivo* as described previously.[24] Dialysis to remove low molecular weight compounds against water using dialysis tubing (12–14K cutoff) over three days yielded cross-linked iron oxide nanoparticles (CLIO). The obtained amine-presenting nanoparticles were then reacted (Figure 1B) with the bifunctional linker, succinimidyl-([*N*-maleimidopropionamido]-4ethyleneglycol)ester (NHS-PEG$_4$-maleimide or SM(PEG)$_4$) in PBS (pH 7.4 buffer). Purification with Microcon® centrifuge filters (10 KDa cutoff, 5 mL -> 0.2 mL volume reduction, 4600 rpm, PBS buffer addition and centrifugation was repeated 5 times) removed low molecular weight compounds to afford cross-linked iron oxide nanoparticles conjugated with the linker-bearing maleimide (CLIO-M).

MMP-14 activatable TNPs were synthesized by conjugating CLIO-M to the peptide-conjugated azademethylcolchicine (ICT). ICT is a modified analogue of the previously reported ICT2588 (currently being progressed towards clinical trials)[12] with an additional cysteine residue at the P5 position to allow conjugation to the nanoparticle via maleimide

(Figure 1). ICT was synthesized using a combination of solution and solid phase peptide synthesis methodologies, and purified by preparative HPLC as previously described.[12] A fully side chain-protected molecule was prepared (ICT3104), to allow convenient storage, transport and to minimize potential cysteine-sulfur oxidation (see supplementary methodology). Side-chain protecting groups were subsequently removed by dissolving ICT3104 (25 mg) in a mixture of TFA: triisopropylsilane (TIS): water (95:2.5:2.5, 1 mL) and stirring at room temperature for 2.5 hours. Following deprotection of ICT3104, the target agent ICT was precipitated with cold diethyl ether (40 mL), centrifuged, resuspended and washed twice with diethyl ether (40 mL). This procedure produced ICT in high yield and purity (13 mg, 91%). Excess of ICT (7 mg/mL, 50:1 molar ratio ICT: CLIO-M nanoparticle) was coupled with CLIO-M in PBS pH 7.4 buffer at room temperature. Purification with Microcon® centrifuge filters (10K cutoff, 5mL -> 0.2mL volume reduction, 4000 rpm, PBS buffer addition and centrifugation) was repeated 10 times until the filtrate had no fluorescence to afford a purified construct, CLIO-ICT.

5.2. Physicochemical Characterization of TNPs

The iron concentrations of all nanoparticle samples were determined by Inductively Coupled Plasma Mass-Spectrometry (ICP-MS) on a Thermo Scientifc XSERIES 2 View Spectrometer. The molar concentration of ferumoxytol was calculated using the concentration of iron determined by ICP-MS and known size of iron oxide core of a NP (6.5 nm on average by TEM ≈ 3600 iron atoms as computed using Diamond® crystal structure analysis software) [24c]. The amount of drug (ICT) covalently linked to a nanoparticle was calculated using two methods. In the first method, FITC (FITC: ICT = 1:1, Table 1) concentration was determined by subtracting the maximum absorption (492 nm) of CLIO-ICT from the absorbance of unconjugated TNP alone (measured for CLIO-NH_2 at the same concentration of iron)[25] and dividing the result by known extinction coefficient of FITC (70,000 M^{-1} cm^{-1}) at 492 nm. In the second method, the FITC's emission peak of a diluted (to avoid fluorescence self-quenching) CLIO-ICT was integrated and its concentration was estimated using a calibration plot obtained for a set of standard FITC solutions. Both methods gave consistent results (less than 8% difference) for three different solutions of CLIO-ICT. TEM samples were prepared by drying 5 μL of 0.5 mM solution on carbon coated 600 mesh copper grid. The samples were imaged on a FEI Tecnai G2 F20 X-TWIN Transmission Electron Microscope at 200kV accelerating voltage. Relativities (r_1 and r_2) were determined by measuring T1 and T2 relaxation times for a series of solutions with iron concentration of 1 – 60 mM on a Varian Inova 300MHz (7 Tesla) NMR spectrometer using a series spin-echo and inversion recovery pulse sequences.

Dynamic Light Scattering (DLS, measures the hydrodynamic radius of the TNP) and Laser Doppler Electrophoresis (measures zeta potential) were performed on a Brookhaven 90 Plus Nanoparticle Size Analyzer. The solutions of nanoparticles in the PBS buffer were filtered via Whatman GD/X 13 Syringe Filter (nylon, 0.2 μm) immediately before measurements. Dilution to 0.6 mM (iron) was required to obtain sufficient number of counts per second due to high value of absorption of TNPs. Absorption spectra were measured in a 1 cm path length cuvette using an Agilent 8453 absorption spectrophotometer. MALDI-MS spectrometric analyses were performed at the Mass Spectrometry Facility of Stanford

University. HPLC was performed on a Dionex HPLC System (Dionex Corporation) equipped with a GP50 gradient pump and an inline diode array UV-Vis detector. A reversed-phase C18 (Phenomenex, 5 μm, 10 × 250 mm or Dionex, 5 μm, 4.6 × 250 mm) column was used with a MeCN (B)/H_2O (A) gradient mobile phase containing 0.1% trifluoroacetic acid at a flow of 3 or 1 mL/min for the analysis.

5.3. *In Vitro* Studies

The murine breast carcinoma MMTV-PyMT (isolated from MMTV-PyMT mouse breast tumors) and 4T1 (ATCC CRL-2539) cell lines and human dermal fibroblasts (ATCC PCS-201-012) were obtained from the American Type Culture Collection and authenticated both morphologically and by short tandem repeat analysis. Cell lines were cultured as monolayers in RPMI 1640 supplemented with 10% (v/v) fetal bovine serum, sodium pyruvate (1 mM), and L-glutamine (2 mM). All cell lines were used at a low passage in our laboratory for a maximum of 6 months post-resuscitation and were tested regularly to confirm lack of Mycoplasma infection.

Assessment of MMP-14 gene expression of MMTV-PyMT and 4T1 tumor cells as well as human dermal fibroblasts as controls was determined by qPCR as previously described.[12] qPCR expression analysis for MMP-14 and the control marker GAPDH was done and the total cellular RNA was extracted from each sample with the QIAGEN RNeasy® mini kit. cDNA was prepared from total RNA and quantitative real-time PCRs (qPCRs) were carried out and analyzed on an Applied Biosystems StepOne™ Real-Time PCR System. The formation of double-stranded DNA product was monitored by TaqMan® gene expression primers.

To monitor stability of CLIO-ICT and ICT, 2 mL of PyMT mouse blood was collected and 100 μL of 0.4 M (Fe) solution of CLIO-ICT and 100 μL 0.29 mM solution of ICT were incubated with 500 μL of fresh blood each at 37 °C for three days. The solutions were filtered via Whatman GD/X 13 Syringe Filter (nylon, 0.2 μm) and analyzed by HPLC, LC-MS and MALDI Mass Spectrometry.

Subsequently, triplicate samples of MMTV-PyMT tumor cells and human dermal fibroblasts were incubated with ferumoxytol, CLIO-ICT, ICT, or PBS, and analyzed for caspase-3 activity levels, a marker of cytotoxicity using the SensoLyte ® Homogeneous AMC Caspase-3/7 assay kit (AnaSpec Inc., California) according to the manufacturer's instructions. Release of the AMC fluorophore following cleavage of the specific fluorometric caspase substrate, DEVD-AMC was detected using a fluorometer (ex/em=354 nm/442 nm).

5.4. *In Vivo* Evaluation of Theranostic Activity

All procedures were approved by the animal care and use committee at Stanford University. MMTV-PyMT mice that spontaneously develop multifocal, multiclonal mammary adenocarcinomas were used.[26] Explants of MMTV-PyMT tumors were implanted into 24 four week old female FvBN mice as described previously.[27] When the tumors had reached a size of 1 cm, four groups of six mice each received a single intravenous injection of 0.5 M (Fe) solution of ferumoxytol (0.5 mmol Fe/kg), 0.4 M (Fe) solution of CLIO-ICT (0.75

mmol Fe/kg and 1 μmol/kg of ICT), 0.29 mM solution of ICT (1 μmol/kg), or PBS (1.0 μl/gm). Due to the approximately 1/3 lower r2-relaxivity of the TNPs compared to the original ferumoxytol, TNPs were administered at a correspondingly higher iron oxide dose. All mice underwent MR imaging on a 1 T desktop MR scanner (Aspect M2™ Compact High Performance MR System, Toronto, ON). Animals were anesthetized with isofluorane and placed in a dedicated radiofrequency coil for high resolution MR imaging, using T2-weighted SE sequences (TR 2500 ms, TE 20, 40, 60, 80 ms) with a field of view (FOV) of 6×6 cm (1T), a matrix of 128×128 pixels and a slice thickness of 1–2 mm. MR scans were obtained directly before, continuously up to 1 hour (h) post injection (p.i.) of ferumoxytol, CLIO-ICT, ICT or PBS, as well as 24 h p.i. T2-relaxation times of the tumor were calculated based on multiecho SE sequences and converted to R2-relaxation rates (R2=1/T2), which are proportional to contrast agent concentration. The relative change in R2 data between pre- and postcontrast MR scans, ΔR2 (%), was determined as a quantitative measurement of tumor contrast enhancement.

5.5. Antitumor Activity

Mice bearing subcutaneous PyMT tumors were randomized into groups (n=6 mice) and received either ferumoxytol, CLIO-ICT, or ICT via intravenous administration. Tumor size (measured by calipers) was recorded daily for 7 days. Tumor diameter and volumes were recorded. Tumor volume was calculated using the formula: $(a^2 \times b)/2$ (a and b are the smaller and larger dimension of the tumor, respectively).

5.6. Histological Assessment of TNPs and Caspase-3 Activity

The distribution of nanoparticles and induction of caspase-3 activity was assessed 48 hours following intravenous administration of TNP and drugs. Mammary tumors and samples of visceral organs were explanted, and placed in Optimal Cutting Temperature (OCT) compound on dry ice for histological processing. For detection of FITC-labeled nanoparticles and therapeutic drugs all slides were mounted using ProLong Gold with DAPI (Invitrogen) and analyzed using an LSM510 confocal microscope (Zeiss, Thornwood, NY). Histologic sections of mammary tumors and visceral organs were stained using standard H&E and iron was detected using DAB-enhanced Prussian Blue staining. Caspase-3 activity was evaluated immunohistochemically by antibody staining of cleaved caspase-3 (Cell Signaling Technology 9661) and Cy3-labeled biotin/avidin detection (Vector Labs and Jackson ImmunoResearch). Labeled cells were analyzed by fluorescence microscopy.

5.7. Statistical Analyses

Quantitative data of experimental groups receiving different diagnostic or therapeutic agents were compared with a Wilcoxon rank sum test and an analysis of variance. $P < 0.05$ was considered significant.

Supplementary Material

Refer to Web version on PubMed Central for supplementary material.

Acknowledgements

The authors thank the Daldrup-Link, Rao and ICL laboratories for critical discussion. This study was supported by grants from NIH/NCI R21CA156124 (to HED), NIH/NCI R01CA140943 (HED), R01CA135294 (JR), R21CA138353A2 (JR), Yorkshire Cancer Research (RAF, JHG and PML), a pilot grant from the Stanford Center for Cancer Nanotechnology Excellence and Translation (CCNE-T; NIH/NCI U54 CA151459), Sanofi-BioX Grant (DWF), and NIH/NCI ICMIC P50 CA114747 (DWF), R01 CA170378 PQ22 (DWF) and NIH R01 CA105102 (DWF). We are thankful to the Stanford Center for Innovation and In-Vivo Imaging (SCI^3) supported by the NCI Cancer Center (P30 CA124435-02) and NCI ICMIC (P50 CA114747) for providing the infrastructure for mice MR imaging.

References

1. a) Myrset G, Couvreur P. Adv Drug Delivery Rev. 2012; 64:1394–1416.b) Jain RK, Stylianopoulos T. Nat Rev Clin Oncol. 2010; 7:653–664. [PubMed: 20838415] c) Lammers T, Kiessling F, Hennink WE, Storm G. Journal of Control Release. 2012, 161:175–187.d) Terreno E, Uggeri F, Aime S. Journal of Control Release. 2012; 161:328–337.
2. Greish K. Cancer Nanotechnology: Methods and Protocols. Grobmyer, M., editor. Vol. 624. 2010. p. 25–37
3. Marcucci F, Lefoulon F. Drug Discov Today. 2004; 9:219–228. [PubMed: 14980540]
4. a) Tozer GM, Prise VE, Wilson J, Cemazar M, Shan SO, Dewhirst MW, Barber PR, Vojnovic B, Chaplin DJ. Cancer Res. 2001; 61:6413–6422. [PubMed: 11522635] b) Tozer GM, Kanthou C, Baguley BC. Nat Rev Cancer. 2005; 5:423–435. [PubMed: 15928673]
5. Reyes-Aldasoro CC, Wilson I, Prise VE, Barber PR, Ameer-Beg SM, Vojnovic B, Cunningham VJ, Tozer GM. Microcirculation. 2008; 15:65–79. [PubMed: 17952797]
6. Kanthou C, Tozer GM. Int J Exp Path. 2009; 90:284–294. [PubMed: 19563611]
7. a) Hinner P, Eskens F, Brit J Cancer. 2007; 96:1159–1165. [PubMed: 17375046] b) van Heeckeren WJ, Wakata S, Cruz J, Duerk J, Cooney MM, Dowlati A, McCrae K, Remick SC. J Clin Onc. 2006; 24:1485–1488.
8. Atkinson JM, Siller CS, Gill JH. Brit J Pharmacol. 2008; 153:1345–1352. [PubMed: 18204490]
9. Coussens LM, Fingleton B, Matrisian LM. Science. 2002; 295:2387–2392. [PubMed: 11923519]
10. a) Ueda J, Kajita M, Suenaga N, Fujii K, Seiki M. Oncogene. 2003; 22:8716–8722. [PubMed: 14647466] b) Sahai E, Ota I, Holmbeck K, Birkedal-Hansen H, Soloway P, Balbin M, Lopez-Otin C, Shapiro S, Inada M, Krane S, Allen E, Chung D, Weiss SJ. Journal of Cell Biol. 2004; 167:769–781. [PubMed: 15557125] c) Devy L, Huang L-L, Naa L, Yanamandra N, Pieters H, Frans N, Chang E, Tao Q, Vanhove M, Lejeune A, van Gool R, Sexton DJ, Kuang G, Rank D, Hogan S, Pazmany C, Ma YJ, Schoenbroodt S, Nixon AE, Ladner RC, Hoet R, Henderikx P, TenHoor C, Rabbani SA, Valentino ML, Wood CR, Dransfield DT. Cancer Res. 2009; 69:1517–1526. [PubMed: 19208838] d) Handsley MM, Edwards DR. Int J Cancer. 2005; 115:849–860. [PubMed: 15729716]
11. Landry R, Jacobs PM, Davis R, Shenouda M, Bolton WK. Am J Nephrol. 2005; 25:400–410. [PubMed: 16088081]
12. Atkinson JM, Falconer RA, Edwards DR, Pennington CJ, Siller CS, Shnyder SD, Bibby MC, Patterson LH, Loadman PM, Gill JH. Cancer Res. 2010; 70:6900–6912. [PubMed: 20663911]
13. a) Elias DR, Thorek DLJ, Chen AK, Czupryna J, Tsourkas A. Cancer Biomark. 2008; 4:287–305. [PubMed: 19126958] b) Kobayashi H, Choyke PL. Accounts Chem Res. 2011; 44:83–90.c) Park J, Yang J, Lim EK, Kim E, Choi J, Ryu JK, Kim NH, Suh JS, Yook JI, Huh YM, Haam S. Angew Chem Int Edit. 2012; 51:945–948
14. Lammers T, Aime S, Hennink WE, Storm G, Kiessling F. Accounts Chem Res. 2011; 44:1029–1038.
15. Villaraza AJL, Bumb A, Brechbiel MW. Chem Rev. 2010; 110:2921–2959. [PubMed: 20067234]
16. Li W, Tutton S, Vu AT, Pierchala L, Li BSY, Lewis JM, Prasad PV, Edelman RR. J Mag Reson Im. 2005; 21:46–52.
17. Lammers T, Rizzo LY, Storm G, Kiessling F. Clin Cancer Res. 2012; 18:4889–4894. [PubMed: 22829203]

18. Cho KJ, Wang X, Nie SM, Chen Z, Shin DM. Clin Cancer Res. 2008; 14:1310–1316. [PubMed: 18316549]

19. a) Olson ES, Jiang T, Aguilera TA, Nguyen QT, Ellies LG, Scadeng M, Tsien RY. P Natl Acad Sci USA. 2010; 107:4311–4316.b) Nguyen QT, Olson ES, Aguilera TA, Jiang T, Scadeng M, Ellies LG, Tsien RY. P Natl Acad Sci USA. 2010; 107:4317–4322.

20. a) Yoo D, Lee JH, Shin TH, Cheon J. Accounts Chem Res. 2011; 44:863–874.b) Ma XW, Zhao YL, Liang XJ. Accounts Chem Res. 2011; 44:1114–1122.c) Kievit FM, Zhang MQ. Accounts Chem Res. 2011; 44:853–862.d) Cabral H, Nishiyama N, Kataoka K. Accounts Chem Res. 2011; 44:999–1008.e) Jokerst JV, Gambhir SS. Accounts Chem Res. 2011; 44:1050–1060.f) Fernandez-Fernandez A, Manchanda R, McGoron AJ. Appl Biochem Biotech. 2011; 165:1628–1651.g) Caldorera-Moore ME, Liechty WB, Peppas NA. Accounts Chem Res. 2011; 44:1061–1070.h) Al-Jamal WT, Kostarelos K. Accounts Chem Res. 2011; 44:1094–1104.

21. a) Ernsting MJ, Foltz WD, Undzys E, Tagami T, Li SD. Biomaterials. 2012; 33:3931–3941. [PubMed: 22369962] b) Liao MY, Lai PS, Yu HP, Lin HP, Huang CC. Chem Commun. 2012; 48:5319–5321.

22. Minelli C, Lowe SB, Stevens MM. Small. 2010; 6:2336–2357. [PubMed: 20878632]

23. a) Balakrishnan VS, Rao M, Kausz AT, Brenner L, Pereira BJG, Frigo TB, Lewis JM. Eur J Clin Invest. 2009; 39:489–496. [PubMed: 19397688] b) Neuwelt EA, Varallyay CG, Manninger S, Solymosi D, Haluska M, Hunt MA, Nesbit G, Stevens A, Jerosch-Herold M, Jacobs PM, Hoffman JM. Neurosurgery. 2007; 60:601–611. [PubMed: 17415196] c) Lu M, Cohen MH, Rieves D, Pazdur R. Am J Hematol. 2010; 85:315–319. [PubMed: 20201089]

24. a) Josephson L, Tung CH, Moore A, Weissleder R. Bioconjugate Chem. 1999; 10:186–191.b) Högemann D, Josephson L, Weissleder R, Basilion JP. Bioconjugate Chem. 2000; 11:941–946.

25. Ziolo RF, Giannelis EP, Weinstein BA, Ohoro MP, Ganguly BN, Mehrotra V, Russell MW, Huffman DR. Science. 1992; 257:219–223. [PubMed: 17794752]

26. a) Vartanovski L, Hollingshead MG, Robles AI, Wu XL, Cherry J, Munroe DJ, Lukes L, Anver MR, Carter JP, Zorgel SD, Stotler H, Bonomi CA, Nunez NP, Harsting SD, Qiao WH, Deng CXX, Green JE, Hunter KW, Merlino G, Steeg PS, Wakefield LM, Barrett JC. Clin Cancer Res. 2007; 13:2168–2177. [PubMed: 17404101] b) Bibby MC. European Journal of Cancer. 2004; 40:852–857. [PubMed: 15120411] c) Kuo TH, Kubota T, Watanabe M, Furukawa T, Kase S, Tanino H, Saikawa Y, Ishibiki K, Kitajima M, Hoffman RM. Anticancer Res. 1993; 13:627–630. [PubMed: 8391244]

27. Guy CT, Cardiff RD, Muller WJ. Mol Cell Biol. 1992; 12:954–961. [PubMed: 1312220] b) Lin EY, Jones JG, Li P, Zhu L, Whitney KD, Muller WJ, Pollard JW. Am J Pathol. 2003; 163:2113–2126. [PubMed: 14578209]

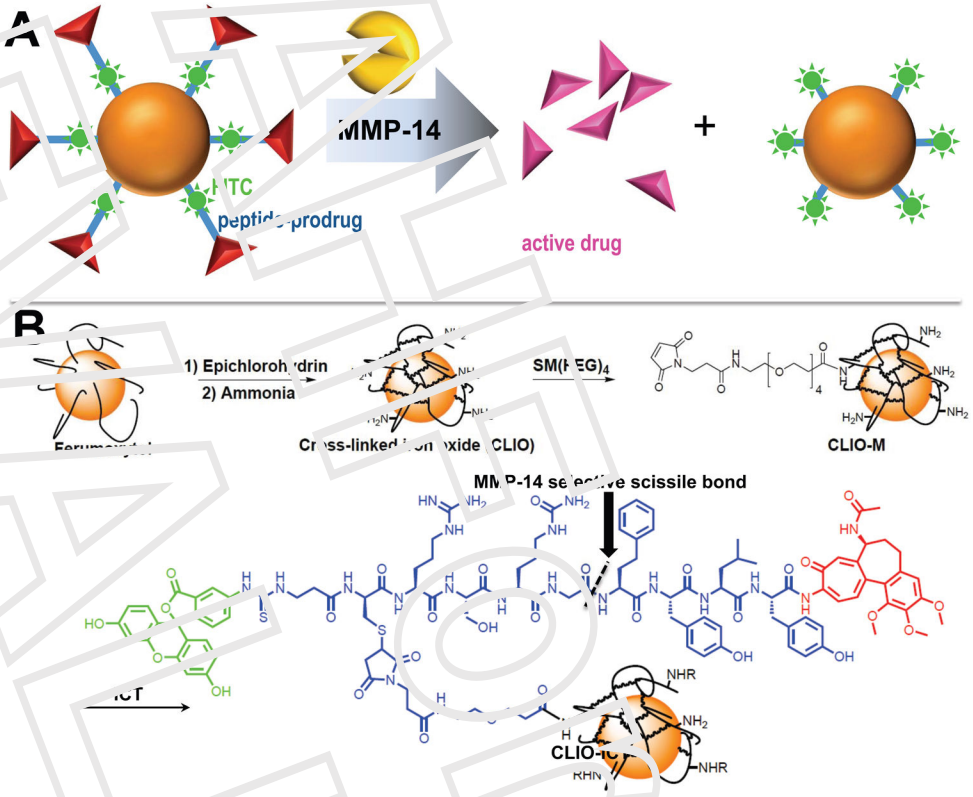

Figure 1.

(A) Schematic representation of theranostic nanoparticle (TNP) activation by MMP-14: the IO NP core is shown in orange; the prodrug ICT is shown in red, and after MMP-14 activation, its product is shown in magenta; the peptide linker is shown in blue, and the FITC is shown in green. **(B)** Synthesis of the theranostic nanoparticle. FITC (shown in green) is linked to the TNP via the amino group of cysteine.

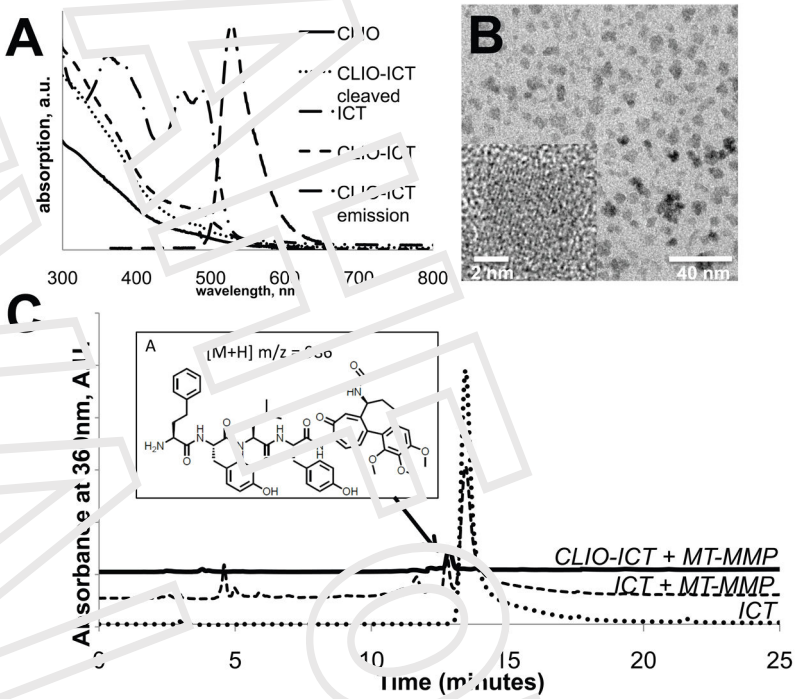

Figure 2.

(A) Absorption spectra of the TNPs and their components (a.u. = arbitrary units) and the emission spectrum of CLIO-ICT (excitation wavelength is 350 nm). ICT absoption is scaled up 5× to avoid the overlap. All spectra recorded at the same ICT emission; Only CLIO (cross-linked iron oxide with amino groups) absorption was measured at the same Fe concentration (0.02 mM) as for CLIO-ICT (ICT concentration is 0.094 mM); **(B)** A representative transmission electron microscopy image of CLIO-ICT. Inset shows crystalline iron oxide core of a single nanoparticle; **(C)** CLIO-ICT activation by MMP-14 in PBS buffer for 30 min and analyzed by HPLC. Mass spectrum of the indicated peak confirmed the presence of product of TNP cleavage by MMP-14. See experimental section for details.

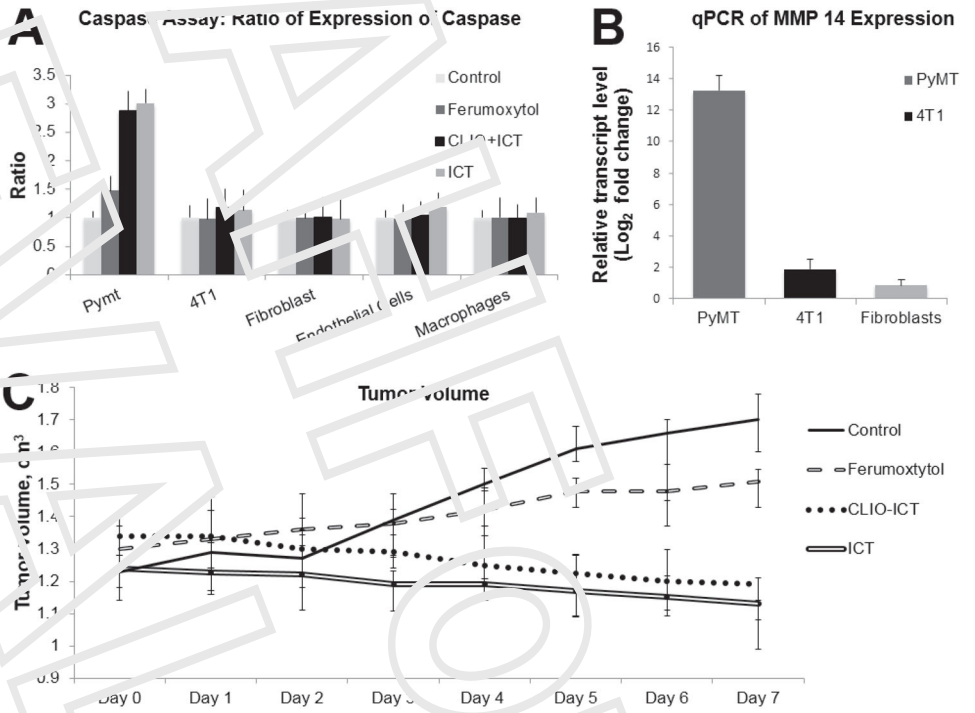

Figure 3.

(A) Caspase assay: PyMT, 4T1, human dermal fibroblasts, endothelial cells, and macrophages were incubated with PBS, Ferumoxytol only, CLIO-ICT, and ICT only. After incubation the assay was run for 4 hr – readings taken every 5 min. Cells incubated with CLIO-ICT along with those incubated with ICT showed more fluorescence (more cell death) than those incubated with Ferumoxytol only and PBS only. Cells incubated with ICT only showed similar levels of fluorescence to that of CLIO-ICT, but showed a plateau after 60 min; **(B)** qPCR of MMP-14 expression of MMTV-PyMT, 4T1 and human dermal fibroblasts; **(C)** PyMT tumor sizes were measured daily for 7 days after intravenous injection of PBS, Ferumoxytol, CLIO-ICT and ICT. The tumor size increases in that of the PBS and Ferumoxytol administered subjects and decreases in the CLIO-ICT and ICT cases. See experimental section for more details.

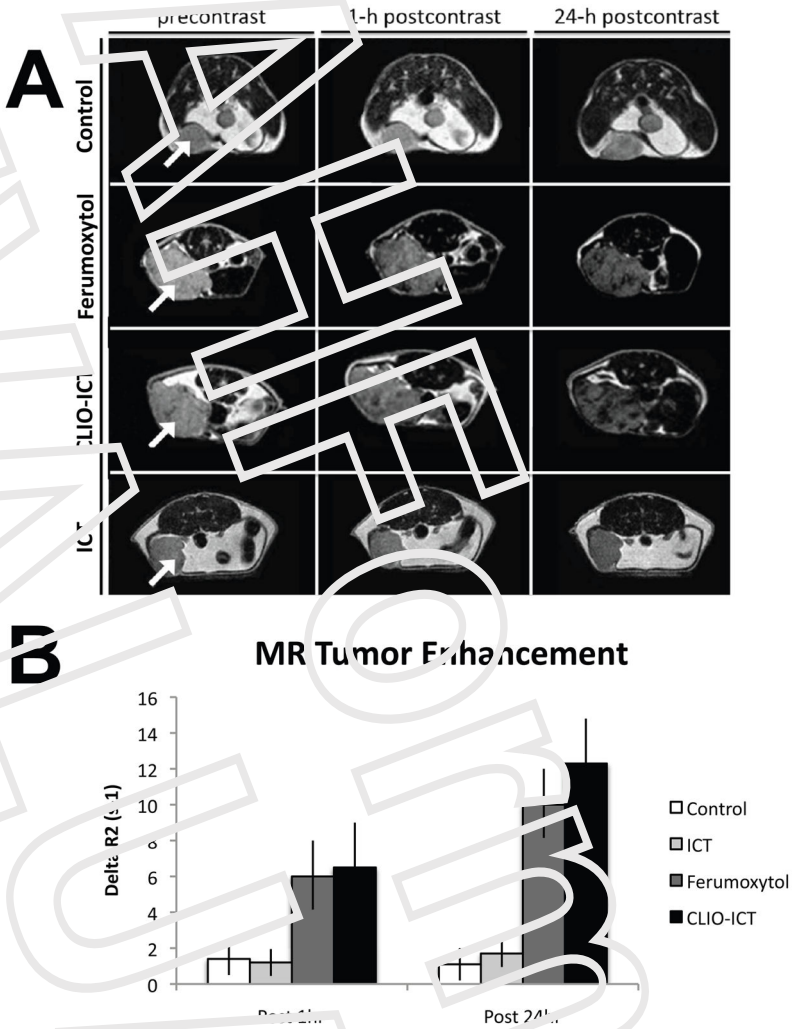

Figure 4.

(A) Axial T2-weighted MR images (TR 2500 ms, TE 80 ms) of MMTV-PyMT mammary tumors before and after a single intravenous injection: 0.6 M (Fe) solution of ferumoxytol (0.5 mmol Fe/kg), 0.4 M (Fe) solution of CLIO-ICT (0.75 mmol Fe/kg and 1.0 μmol/kg of ICT), 0.29 mM solution of ICT (1.0 μmol/kg), or PBS(1.0 ml/gm). Contrast agent accumulation is noted as a negative (dark) signal enhancement of the tumors; **(B)** MR signal enhancement data in tumors corresponding to Figure 4 quantified as $\Delta R_2 = (R_2pre - R_2post)$. Data are displayed as mean data of n=6 tumors in each group for 1h and 24h time points.

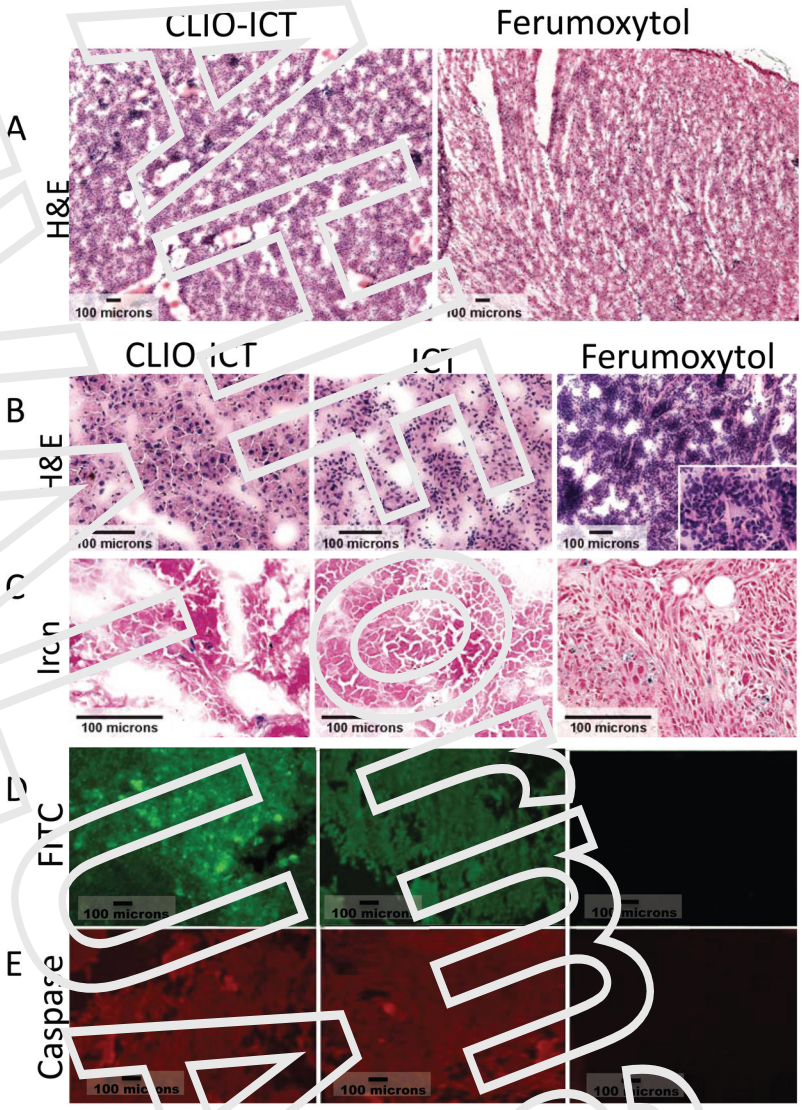

Figure 5.

(A) MMP-14 negative fibroblasts: H&E stained histologic sections of fibroblasts treated with CLIO-ICT and ICT showing no necrosis (both images taken at 40X magnification); **(B)** TNP-induced cell death in MMTV-PyMT tumors. H&E panels: CLIO-ICT treated tumor demonstrating diffuse necrosis (200X magnification); ICT treated tumor with predominately viable tumor cells and a subset of cells undergoing necrosis (200X magnification); Ferumoxytol treated tumor with diffuse viability and no necrosis (100X magnification, inset: 400X magnification); **(C)** Iron panels: Scattered CLIO-ICT treated tumor and rare admixed histiocytes contain blue pigment indicating cytoplasmic iron deposition (200X magnification); ICT treated tumor shows no cytoplasmic iron deposition, scattered iron laden histiocytes serve as an internal positive control (200X magnification). Ferumoxytol treated tumor show cytoplasmic iron deposition, scattered iron laden histiocytes serve as an internal positive control (200X magnification). **(D)** fluorescence microscopy showing FITC signal for CLIO-ICT and ICT but no signal for Ferumoxytol. **(E)** Caspase-3 panels

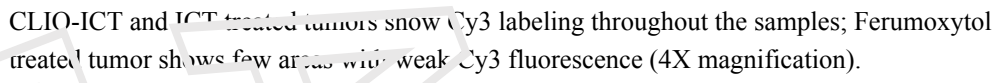

CLIO-ICT and ICT treated tumors show Cy3 labeling throughout the samples; Ferumoxytol treated tumor shows few areas with weak Cy3 fluorescence (4X magnification).

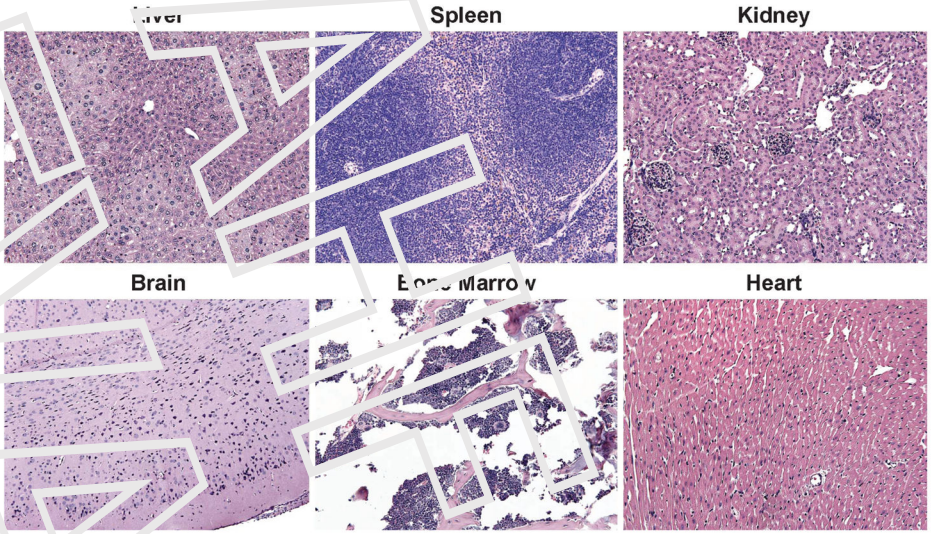

Figure 6.

CLIO-cRGDs do not cause toxic effects in normal organs. Above histopathologies show no significant necrosis of normal organs on H&E staining of the Heart, Kidney, Spleen, Brain, Bone Marrow and Liver.

Table 1

Theranostic Nanoparticles characterization summary. See experimental section for details.

	D, nm (DLS)	Z, meV	# of ICT	r_1/r_2, mM^{-1} s^{-1}
Feraimoxytol	19±4	−13±5		32.3/74.9
CLIO-ICT	21±3	+21±7	4.7±0.4	38.9/57.0
CLIO-ICT cleaved	19±4	+16±6	0.6±0.2	39.5/55.2